Does eddy-eddy interaction control surface phytoplankton distribution and carbon export in the North Pacific Subtropical Gyre?

Lionel Guidi,[1,2] Paulo H. R. Calil,[2,3,4] Solange Duhamel,[1,2,5] Karin M. Björkman,[1,2] Scott C. Doney,[2,3] George A. Jackson,[6] Binglin Li,[1,2] Matthew J. Church,[1,2] Sasha Tozzi,[2,7,8] Zbigniew S. Kolber,[2,7,8] Kelvin J. Richards,[1,2] Allison A. Fong,[1,2] Ricardo M. Letelier,[2,9] Gabriel Gorsky,[10] Lars Stemmann,[10] and David M. Karl[1,2]

[1] In the North Pacific Subtropical Gyre (NPSG), the regular occurrence of summer phytoplankton blooms contributes to marine ecosystem productivity and the annual carbon export. The mechanisms underlying the formation, maintenance, and decay of these blooms remain largely unknown; nitrogen fixation, episodic vertical mixing of nutrients, and meso- (<100 km) and submesoscale (<10 km) physical processes are all hypothesized to contribute to bloom dynamics. In addition, zones of convergence in the ocean's surface layers are known to generate downwelling and/or converging currents that affect plankton distributions. It has been difficult to quantify the importance of these convergence zones in the export flux of particulate organic carbon (POC) in the open ocean. Here we use two high-resolution ocean transects across a pair of mesoscale eddies in the vicinity of Station ALOHA (22° 45′N, 158° 00′W) to show that horizontal turbulent stirring may have been a dominant control on the spatial distribution of the nitrogen fixing cyanobacterium *Trichodesmium* spp. Fast repetition rate fluorometry measurements suggested that this distribution stimulated new primary production; this conclusion was not confirmed by ^{14}C-based measurements, possibly because of different sampling scales for the two methods. Our observations of particle size distributions along the two transects showed that stretching by the mesoscale eddy field produced submesoscale features that mediated POC export via frontogenetically generated downwelling currents. This study highlights the need to combine high-resolution biogeochemical and physical data sets to understand the links between *Trichodesmium* spp. surface distribution and POC export in the NPSG at the submesoscale level.

1. Introduction

[2] The North Pacific Subtropical Gyre (NPSG) is the largest continuous biome on Earth. The warm, oligotrophic surface waters of the NPSG support substantial export of organic carbon [*Martin et al.*, 1987; *Emerson et al.*, 1997]. Despite vanishingly low surface inorganic nutrient concentrations, late summer phytoplankton blooms are a recurrent feature of this ecosystem [*Dore et al.*, 2008]. These seasonal blooms occur between June and October, when the upper ocean warms to 25°–27°C, the mixed layer shoals (<70 m), and the surface concentrations of inorganic nutrients are at their annual minima. The phytoplankton often include elevated abundances of nitrogen fixing cyano-bacteria, including buoyant *Trichodesmium* spp. colonies

[1]Department of Oceanography, University of Hawai'i at Manoa, Honolulu, Hawai'i, USA.

[2]Center for Microbial Oceanography: Research and Education (C-MORE), University of Hawai'i at Manoa, Honolulu, Hawai'i, USA.

[3]Department of Marine Chemistry and Geochemistry, Woods Hole Oceanographic Institution, Woods Hole, Massachusetts, USA.

Corresponding author: L. Guidi, CNRS/Laboratoire d'Océanographie de Villefranche sur Mer, 181 Chemin du Lazaret, BP 28, Villefranche-sur-Mer, Alpes Maritimes, FR-06234, France. (lguidi@obs-vlfr.fr)

[4]Now at Instituto de Oceanografia, Universidade Federal do Rio Grande, Rio Grande, Brazil.

[5]Now at Division of Biology and Paleoenvironment, Lamont-Doherty Earth Observatory, Palisades, New York, USA.

[6]Department of Oceanography, Texas A&M University, College Station, Texas, USA.

[7]Monterey Bay Aquarium Research Institute, Moss Landing, California, USA.

[8]Ocean Sciences, University of California, Santa Cruz, California, USA.

[9]College of Oceanic and Atmospheric Sciences, Oregon State University, Corvallis, Oregon, USA.

[10]CNRS/Université Pierre et Marie Curie–Paris 6, Laboratoire d'Océanographie de Villefranche, Villefranche-sur-Mer, France.

(see below for definition) and/or diatom-cyanobacteria symbioses of *Rhizosolenia-Richelia* and *Hemiaulus-Richelia* [*Letelier and Karl*, 1996; *Wilson*, 2003; *White et al.*, 2007; *Fong et al.*, 2008; *Church et al.*, 2009]. The surface ocean expression of summer blooms is characterized by meso- (<100 km) and submesoscale (<10 km) patches of elevated chlorophyll [*Dore et al.*, 2008]. The biological and physical mechanisms structuring the spatial variability and modulating the new production and export flux from these blooms are poorly understood.

[3] Episodic upwelling events associated with mesoscale eddies can inject nutrients into the euphotic layer of the NPSG and thus drive new production and export [*Letelier et al.*, 2000]. These events have been estimated to transport an average of 0.088 mol N m^{-2} y^{-1} into the euphotic zone of the NPSG [*Johnson et al.*, 2010]. Model estimates for the subtropical North Atlantic indicate that similar mesoscale processes contribute about 0.14 mol N m^{-2} y^{-1} there [*Oschlies and Garçon*, 1998; *McGillicuddy et al.*, 2003]. More recently, it has been suggested that large vertical velocities associated with submesocale structures could be responsible for the injection of an additional 0.12 mol N m^{-2} y^{-1}, doubling the estimated subtropical nutrient inputs and potentially closing the total nutrient budget [*Mahadevan and Archer*, 2000; *Lévy et al.*, 2001; *Lapeyre and Klein*, 2006]. In addition, it has been suggested that mesoscale features could stimulate dinitrogen (N$_2$) fixation, another form of new production, by bringing other nutrients to the upper ocean, a mechanism that would favor *Trichodesmium* spp. and *Richelia* growth [*Davis and McGillicuddy*, 2006; *Church et al.*, 2009]. These organisms could in turn enhance primary production by releasing new nitrogen in the euphotic layer, allowing an increase of carbon export from other phytoplankton species [*Moore et al.*, 2006].

[4] Horizontal stirring, associated with eddies and filaments, affects the spatial distribution of plankton blooms and may even determine phytoplankton community structure and dominant groups by creating fluid dynamical niches within scales of a few kilometers [*Abraham*, 1998; *d'Ovidio et al.*, 2010]. Such spatial heterogeneity leads to spatial variability in carbon export [*Guidi et al.*, 2007]. While modeling studies tend to support this hypothesis [*Klein and Lapeyre*, 2009; *Lévy et al.*, 2009; *Calil and Richards*, 2010], few in situ data are available, mainly because of limitations of common instrumentation in capturing spatial variability of carbon export [*Guidi et al.*, 2007; *Niewiadomska et al.*, 2008].

[5] Our study investigates these mechanisms by combining meso- and submesoscale in situ observations and modeling analyses of the NPSG ecosystem. We employ a multidisciplinary approach, with a suite of biogeochemical and hydrographic measurements, to study the evolution of a *Trichodesmium* spp. bloom. The data were collected around Station ALOHA (22° 45′N, 158° 00′W) during the Ocean PERturbation EXperiment (OPEREX) cruise in summer 2008 (Figure 1). We show that horizontal stirring, resulting from the interaction of two relatively weak mesoscale eddies (a cyclone and an anticyclone), appeared to control the distribution of phytoplankton biomass around these features. We argue that surface frontogenesis-induced downwelling in the frontal region between the two eddies which, along with horizontal convergence, increased particulate organic carbon

(POC) export. Through a description of the spatial distribution of particles and *Trichodesmium* spp., together with analysis of the particle size distributions, our study provides additional insight into mechanisms promoting phytoplankton blooms and export in the NPSG.

2. Methods

2.1. Instrumentation and Sample Analysis

[6] Hydrographic and biogeochemical data, including temperature, salinity, fluorescence, beam attenuation (transmissometer, λ = 660 nm, 25 cm path length), and dissolved oxygen (CTD/rosette package), were measured in situ or in seawater samples at all stations. In addition, pigments were analyzed using high-performance liquid chromatography (HPLC) at 13 stations spanning the eddy field (7 in the anticyclone, 4 in the cyclone and 2 in the front). All seawater biogeochemical analyses followed the Hawaii Ocean Time-series (HOT) analytical methods protocols. Detailed description of all methods can be found on the HOT Web site: http://hahana.soest.hawaii.edu/hot/methods/results.html.

[7] Fluorescence signals (amplitude, F_v/F_m ratio, and functional absorption cross section) were measured by fast repetition rate fluorometry (FRRF) along a 70 km transect across the frontal zone (i.e., the region between eddies). Carbon fixation was estimated using photosynthesis versus irradiance relationships for samples from near-surface depths (5 m) and from the deep chlorophyll maximum (DCM) in the anticyclone, cyclone, and frontal zones; photosynthetic parameters were computed using the negative exponential formulation described in *Platt et al.* [1980].

[8] Picoplankton (bacterioplankton, *Prochlorococcus*, *Synechococcus* and picophytoeukaryotes) were counted in preserved samples from 11 stations across the eddy field using a Cytopeia Influx Mariner flow cytometer. Samples were fixed with paraformaldehyde (final concentration of 0.2%) immediately after sampling, flash frozen in liquid nitrogen, and stored at −80°C until analyzed (within 4 months). Pigmented groups (*Prochlorococcus*, *Synechococcus* and picophytoeukaryotes) were enumerated in unstained samples. *Prochlorococcus* and picophytoeukaryotes were characterized using their natural chlorophyll fluorescence; their lack of phycoerythrin was used to discriminate them from *Synechococcus*. Bacterioplankton were counted after staining with a 1 ml aliquot of SYBR Green I DNA dye (0.01% final concentration). Because of the overlap in forward scattering and fluorescence for bacterioplankton and *Prochlorococcus* groups after staining with SYBR Green I, bacterioplankton abundance in surface samples was calculated by subtracting *Prochlorococcus* abundance determined in the unstained aliquot from the SYBR Green I stained picoplankton abundances. Flow cytometry data were analyzed with the FlowJo 7 software (Tree Star, Inc.). To compare the data between samples, an internal standard of 1 μm microspheres (Fluoresbrite, Polysciences) was added to each sample.

[9] Carbon flux was measured using free-drifting sediment traps [particle-interceptor-traps style; *Knauer et al.*, 1979] deployed at 150 and 300 m depth in the frontal zone and in the center of the cyclone, and particle abundance and size distribution were measured using an Underwater Vision
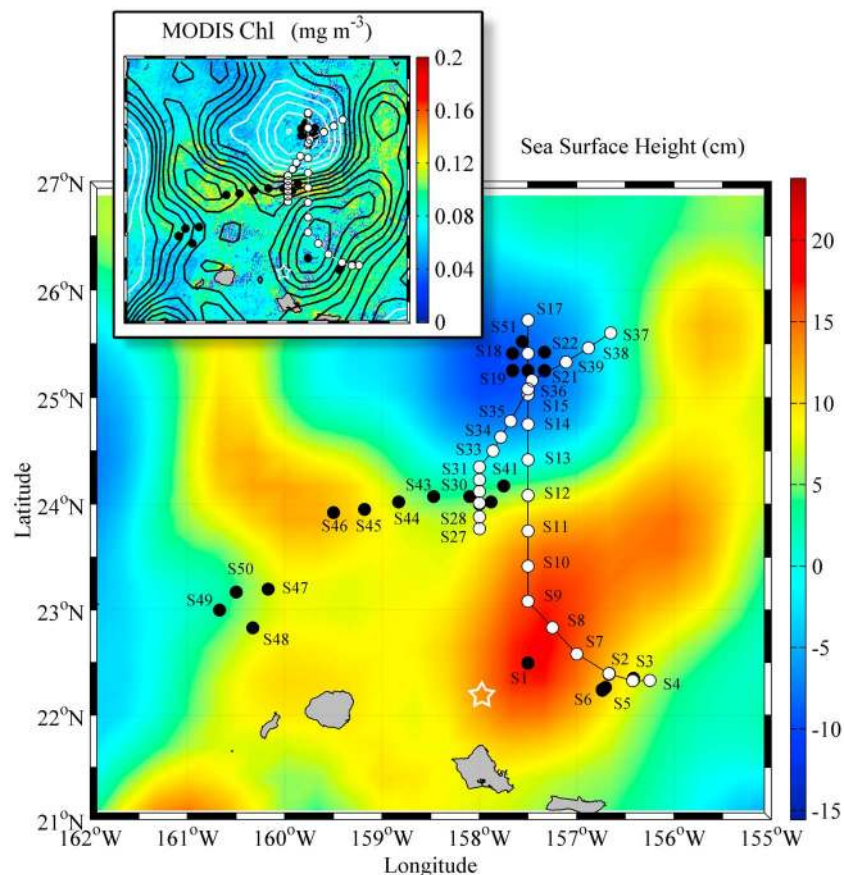
Figure 1. Station locations from the OPEREX cruise track superimposed on the AVISO-derived sea surface height (SSH) anomaly (6 August 2008). The same stations are plotted over the MODIS-derived chlorophyll *a* measurements (8-day composite centered on 5 August 2008) in the upper left corner with AVISO SSH superimposed (white lines representing cyclonic circulation and black lines for anticyclonic circulation). Solid white symbols denote the 2 transects (Transect 1, including stations 2–17, passing through the anticyclone and cyclone with a spatial resolution of 37 km; Transect 2, including stations 27–37, passing through the frontal zone and the cyclone with a spatial resolution of 13 km in the frontal zone). Solid black symbols represent the stations used for the survey and for more comprehensive biogeochemical analyses. The white star marks the location of Station ALOHA. The first sediment trap was deployed (25.08°N, 157.50°W) and recovered (25.63°N, 157.54°W) in the center of the cyclone, while the second was deployed (24.00°N, 158°W) and recovered (24.22°N, 157.48°W) within the frontal zone.

Profiler (UVP5) [*Picheral et al.*, 2010] deployed at all stations.

2.2. *Trichodesmium* spp. Abundances and Sinking Flux

[10] A *Trichodesmium* spp. colony is generally formed of ∼200 trichomes, and each trichome contains ∼100 cells [*Carpenter*, 1983; *Letelier and Karl*, 1996; *LaRoche and Breitbarth*, 2005; *Benavides et al.*, 2011]. In this study, the UVP5 was used to estimate the distribution of *Trichodesmium* spp. colonies and microscopy was used to count trichomes per colony. A molecular approach was used to estimate the sinking flux of *Trichodesmium* spp. cells.

[11] *Trichodesmium* spp. colony abundances between the surface and 120 m (base of the euphotic layer) were estimated using the UVP5 and semi-automatic identification of the particles >500 μm followed by visual validation of all sorted images [for details, see *Picheral et al.*, 2010].

[12] Samples for enumeration of *Trichodesmium* spp. trichomes were collected at 5, 25, 45, and 75 m depth. Seawater (12 L) was filtered by gravity directly from the rosette sampling bottles onto 47 mm diameter, 2 μm porosity polycarbonate filters held by inline filter holders. Filters were fixed with 2% paraformaldehyde, then mounted onto glass microscopy slides (50 × 75 mm, GOLD SEAL®) with Type FF immersion oil (Cargille Laboratories) and covered (Fisher brand 45 × 50 mm coverslips). Slides were frozen at −20°C until trichomes were enumerated in the laboratory by epifluorescence microscopy (Zeiss Observer Z1).

[13] Sinking flux of *Trichodesmium* spp. in detrital material was estimated using results from amplification of diazotroph *nifH* genes collected from sediment trap samples at 150 and 300 m. The trap solutions were pressure filtered onto 47 mm diameter, 2 μm porosity polycarbonate filters. DNA was extracted from the filters using a combined cetyltrimethylammonium bromide-chloroform method [*Zhang*

and Lin, 2005]. The number of *Trichodesmium* spp. *nifH* gene copies was estimated based on a quantitative polymerase chain reaction (qPCR) assay described in *Church et al.* [2005].

2.3. POC Flux From Particle Size

[14] Particulate organic carbon flux was estimated from the knowledge of particle size distributions (P) and concentration as a function of particle diameter (d) [*Jackson et al.*, 1997]. The total mass flux (F) was calculated by integrating the size-specific flux $P(d)m(d)w(d)$ over all particle sizes, using the diameter as a measure of particle size:

$$F = \int_{0}^{\infty} P(d)m(d)w(d)\mathrm{d}d \tag{1}$$

where F is the total particle mass flux, m is the particle mass and w is the particle settling rate. The particle flux was estimated using an approximation of equation (1) over a finite number (x) of small logarithmic intervals for diameter d spanning from 250 μm to 1.5 mm. Particles <250 μm and >1.5 mm were not considered, consistent with the method presented by *Guidi et al.* [2008]. Assuming that particle mass and settling rate were related to diameter by a power law [*McCave*, 1984; *Alldredge and Gotschalk*, 1988; *Guidi et al.*, 2008], $m(d)w(d) = Ad^b$, equation (1) can be approximated by:

$$F = \sum_{i=1}^{x} P_i \cdot A \cdot d_i^b \tag{2}$$

[15] The empirical power law coefficient A and exponent b and their standard deviations have previously been estimated using a minimization procedure matching a global data set of 118 particle size distributions from UVPs and particle mass fluxes measured from nearby sediment traps [see *Guidi et al.*, 2008 for details]. These parameters were $A = 109.5 \pm 32.6$ mg m^{-2-b} d^{-1} and $b = 3.52 \pm 0.72$. Particle composition varies regionally within the ocean, and we therefore calculated a regional POC:mass flux ratio based on sediment trap measurements from the HOT program data record, 1988–1995. The POC:mass flux ratios (median, 1st and 3rd quartiles) were used to convert mass fluxes, calculated based on the particle size distribution (equation (2)), to POC fluxes. Error estimates for the particle size distribution based POC fluxes were derived using the reported errors on the A and b coefficients [*Guidi et al.*, 2008] and quartiles from the POC:mass flux ratio at Station ALOHA.

2.4. Modeling Experiment of Float Advection and FSLE Calculation

[16] We assessed the mesoscale physical circulation for the OPEREX region using sea surface height anomalies derived from satellite altimetry. Using the resulting surface geostrophic velocity estimates in numerical model experiments, we explored the impact of mesoscale circulation on biological distributions. In particular, we analyzed the trajectories of synthetic floats (i.e., virtual particles) seeded into the model domain using the backward finite-size Lyapunov exponent (FSLE) technique, which has been used in recent studies to understand the control exerted by horizontal

stirring on the spatial distribution of surface ocean tracers including sea surface temperature and chlorophyll *a* [*d'Ovidio et al.*, 2004; *Lehahn et al.*, 2007; *Calil and Richards*, 2010]. The information contained in the FSLEs permit estimations of the time-scales of horizontal stirring and regions of surface frontogenesis, where sharpening of surface density gradients is often associated with strong vertical velocities on the submesoscale [*Lehahn et al.*, 2007; *Calil and Richards*, 2010; *Calil et al.*, 2011].

[17] Regions of frontogenesis are marked by rapid particle dispersion and stirring. Specifically, the FSLE fields are computed by advecting pairs of synthetic floats whose initial separation distances are arbitrarily small and then measuring the change in separation distance between floats as a function of time. Rapidly growing separation distances indicate areas of stronger dispersion and larger values of the backward FSLE's. We used an initial separation distance of 1 km and advected synthetic floats using surface geostrophic velocities estimated from the Archiving, Validation and Interpretation of Satellite Oceanographic (AVISO) data. We tracked float trajectories until separations reached a stopping size of 60 km, which is roughly characteristic of the scale of eddies in this region based on satellite altimetry and ocean color data [*Doney et al.*, 2003]. The inverse of the time required to reach the separation distance, proportional to the FSLE, was mapped onto the geographic coordinates of the initial positions of the floats. Float pairs whose separation was smaller than 60 km at the end of the total integration time (100 days) had their FSLEs set to zero [see *Calil et al.*, 2011 for details].

3. Results

3.1. Study Site and Physical Characteristics

[18] During the 15 day long OPEREX cruise (30 July to 14 August 2008), the dominant physical feature near Station ALOHA was a sea surface topography dipole, with a cyclonic eddy to the north, an anticyclonic eddy to the south, and a transition region between them designated as the frontal zone (Figure 1). The analysis of sea surface height anomaly fields showed that this dipole was relatively stable in intensity and propagated westward at an average speed of 4 km d^{-1} over the observation period. Sample profiles (0–300 m) within this region were collected during two ship transects through the dipole; the first one took place between 2 and 5 August, and the second occurred from 6 to 9 August. There were 14 stations spaced 37 km apart in the first transect and 14 stations spaced 13 km apart in the second.

3.2. Nutrient Field

[19] Upper ocean nutrient distributions across the eddy field, starting from the south within the anticyclone then moving north through the frontal zone and into the cyclonic feature, showed the characteristic doming of the isopycnal surfaces within the cyclonic eddy with higher nutrient concentrations closer to the surface than in either the anticyclone or the frontal regions (Figure 2). The nitrate + nitrite (N+N) 0–200 m inventory progressively increased northward along the transect (N+N vertically integrated inventory mmol m^{-2}: 81 ± 33, 135 ± 10 and 287 ± 46 in the anticyclone, frontal zone, and cyclone, respectively) (Figure 2a and Table 1). In contrast, the depth integrated inventories (0–200 m) of
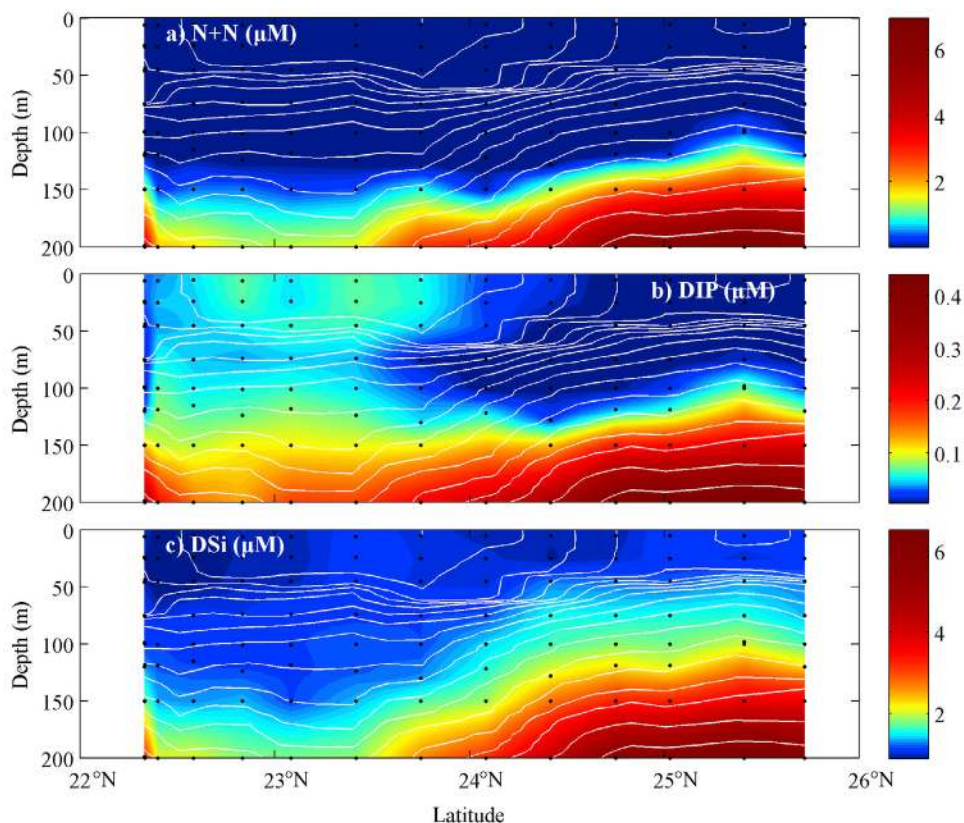
Figure 2. Nutrient field with white contours plot of the density field from the southern anticyclone, through the frontal zone and into the cyclonic feature to the north. Concentrations of (a) nitrate + nitrite, (b) dissolved inorganic phosphorus, and (c) dissolved silicate.

dissolved inorganic phosphorus (DIP) were relatively similar in the anticyclone and frontal zones, but significantly higher within the cyclone (DIP vertically integrated inventory mmol m^{-2}: 15.9 ± 1.2, 14.3 ± 0.7 and 23.0 ± 2.7) (Figure 2b and Table 1). The N+N:DIP ratios of these inventories also progressively increased from the anticyclone to the cyclone, although never reaching the Redfield ratio of 16 [*Redfield et al.*, 1963]. The uppermost water column had low inventories in both N+N and DIP, typical for this subtropical gyre environment (Sta. ALOHA) [*Karl et al.*, 2001]; however, the 0–45 m DIP was considerably more depleted within the cyclone compared to the other regions sampled (0–45 m, DIP vertically integrated inventory mmol m^{-2}: 2.3 ± 0.7, 1.0 ± 0.4 and 0.3 ± 0.0l) (Table 1) resulting in slightly increased N+N:DIP ratios in that depth range within the cyclone relative to the anticyclone and frontal zone stations. Dissolved silicate (DSi) inventories (0–200 m) also increased with the doming isopycnals within the cyclone (DSi mmol m^{-2}: 270 ± 23, 374 ± 65 and 506 ± 29) (Figure 2c and Table 1). However, the upper water column did not show large differences among the three regions (0–45 m, DSi mmol m^{-2}: 46 ± 4, 48 ± 0 and 52 ± 2) (Table 1).

3.3. Spatial Distribution of *Trichodesmium* spp.

[20] Microscopic observations of the phytoplankton community larger than 2 μm revealed that the upper 75 m of the water column within the frontal zone was characterized by relatively high abundances of the nitrogen-fixing cyanobacterium *Trichodesmium* spp. (3.69 × 10^6 trichomes m^{-2}) (Table 1) compared to the abundances in the two eddies (9.75 × 10^5 and 7.65 × 10^5 trichomes m^{-2} in the anticyclone and cyclone, respectively). The high concentrations of *Trichodesmium* spp. in the frontal region were confirmed using images from the UVP5. Stations from the 2 transects and neighboring stations were sorted into 5 sub-regions as a function of latitude using sea surface height anomaly in order to visually select their limits: edge of the anticyclone *(n = 12; 22–22.5°N)*, anticyclone (*n* = 9; 22.5–23.7°N), front (*n* = 19; 23.7–24.3°N), cyclone (*n* = 19; 24.3–25.5°N), and edge of the cyclone (*n* = 2; 25.5–26°N). The differences between the sub-regions were tested with a Kruskal-Wallis nonparametric one-way ANOVA (Figure 3). There were significant differences in the medians of the integrated *Trichodesmium* spp. colony abundance (p < 0.001) (Figure 3). Moreover, the integrated abundance in the front was significantly greater than in the cyclone and the anticyclone (22.2 × 10^3 versus 2.5 × 10^3 and 10.1 × 10^3 colonies m^{-2}) (Table 1). Integrated total POC (0–100 m) from the anticyclone, through the front, to the cyclone remain relatively constant (28.6, 33.3, and 30.8 mgC m^{-2} respectively) (Table 1). Assuming a *Trichodesmium* spp. carbon content equal to 42 pgC cell^{-1} [*Goebel et al.*, 2008], the contributions of *Trichodesmium* spp. to the total POC for the anticyclone, front, and cyclone would be equal to 2.2%, 5.1% and 0.9%, respectively.

Table 1. Summary of the Biogeochemical Composition of the Anticyclone, Front, and Cyclone Water Column During the OPEREX Cruise[a]

	Anticyclone	Front	Cyclone
DIP (Integrated 0–200 m in mmol m^{-2})	15.9 ± 1.2 ($n = 7$)	14.3 ± 0.7 ($n = 2$)	23.0 ± 2.7 ($n = 4$)
DIP (Integrated 0–45 m in mmol m^{-2})	2.3 ± 0.7 ($n = 7$)	1.0 ± 0.4 ($n = 2$)	0.3 ± 0.0 ($n = 4$)
N + N (Integrated 0–200 m in mmol m^{-2})	81 ± 33 ($n = 7$)	135 ± 10 ($n = 2$)	287 ± 46 ($n = 4$)
DSi (Integrated 0–200 m in mmol m^{-2})	270 ± 23 ($n = 7$)	374 ± 65 ($n = 2$)	506 ± 29 ($n = 4$)
DSi (Integrated 0–45 m in mmol m^{-2})	46 ± 4 ($n = 7$)	48 ± 0 ($n = 2$)	52 ± 2 ($n = 4$)
POC (Integrated 0–100 m in mgC m^{-2})	28.6 ($n = 1$)	33.3 ($n = 1$)	30.8 ($n = 1$)
Fucoxanthin (Integrated 0–75 m in μg m^{-2})	628 ± 225 ($n = 7$)	335 ± 130 ($n = 2$)	391 ± 85 ($n = 4$)
Prochlorococcus (Integrated 0–150 m in × 10^{13} cell m^{-2})	2.65 ± 0.17 ($n = 4$)	2.38 ± 0.22 ($n = 3$)	2.35 ± 0.29 ($n = 4$)
Bacterioplankton (Integrated 0–150 m in × 10^{13} cell m^{-2})	7.21 ± 0.69 ($n = 4$)	7.03 ± 0.45 ($n = 3$)	7.18 ± 0.7 ($n = 4$)
Picophytoeukaryotes (Integrated 0–150 m in × 10^{11} cell m^{-2})	1.42 ± 0.09 ($n = 4$)	1.72 ± 0.22 ($n = 3$)	1.84 ± 0.27 ($n = 4$)
Synechococcus (Integrated 0–150 m in × 10^{11} cell m^{-2})	1.56 ± 0.26 ($n = 4$)	1.41 ± 0.05 ($n = 3$)	1.77 ± 0.33 ($n = 4$)
Copepods (Integrated 0–120 m in # m^{-2})	698 ± 517 ($n = 9$)	722 ± 712 ($n = 19$)	1312 ± 586 ($n = 19$)
Trichome counts from slides (0–75 m in # m^{-2})	9.75 × 10^5 ($nr = 3$)	3.69 × 10^6 ($nr = 3$)	7.65 × 10^5 ($nr = 3$)
nifH genes flux (150 m in m^{-2} d^{-1})	–	8.3 ± 1.3 × 10^6 ($nr = 2$)	6.2 ± 0.4 × 10^5 ($nr = 2$)
nifH genes flux (300 m in m^{-2} d^{-1})	–	4.7 ± 0.8 × 10^6 ($nr = 2$)	1.9 ± 0.9 × 10^5 ($nr = 2$)
Trichodesmium colonies from UVP (0–120 m in # × 10^3 m^{-2})	6.8 < 10.1 < 12.7 ($n = 9$)	13.5 < 22.2 < 30.6 ($n = 19$)	1.6 < 2.5 < 7.2 ($n = 19$)
Sediment trap carbon flux (150 m in mg m^{-2} d^{-1})	–	26.4 ± 2.7 ($nr = 3$)	15.2 ± 3.8 ($nr = 3$)
Sediment trap carbon flux (300 m in mg m^{-2} d^{-1})	–	14.7 ± 1.3 ($nr = 3$)	10.6 ± 1.6 ($nr = 3$)
UVP size-based carbon flux (150 m in mg m^{-2} d^{-1})	1.1 < 9.5 < 28.3 ($n = 9$)	2.9 < 11.0 < 32.8 ($n = 19$)	0.4 < 5.1 < 15.9 ($n = 19$)
UVP size-based carbon flux (300 m in mg m^{-2} d^{-1})	1.0 < 4.5 < 13.6 ($n = 4$)	1.3 < 5.4 < 15.3 ($n = 12$)	0.5 < 2.2 < 6.3 ($n = 10$)

[a]The general format used is mean ± standard deviation, first quartile < median < third quartile for UVP5 *Trichodesmium* spp. counts, and UVP5 flux minimum < mean < maximum; *n* is the number of stations available for each parameter, and *nr* the number of replicates (one deployment with multiple traps for the sediment traps and one station with multiple slides counts for *Trichodesmium* spp. trichome counts).

3.4. Biogeochemistry Spatial Variability

[21] Surface chlorophyll *a* concentrations derived from the Moderate Resolution Imaging Spectroradiometer (MODIS) satellite observations were greater in the frontal zone (Figure 1). In situ fluorescence revealed the presence of a DCML. In the cyclone, the DCML shoaled, intensified, and reached a maximum value of 0.9 ± 0.3 mg m^{-3} near 90 m compared to 0.5 ± 0.1 mg m^{-3} near 100 m for the rest of the region (Figure 4a). The concentration of small particles, determined by its effects on transmissivity ($\lambda = 660$ nm), indicated particle accumulation between 0 and 100 m in the frontal zone and along the southern edge of the anticyclone

(Figure 4b). This is consistent with the locations of surface chlorophyll *a* patches sensed by MODIS (Figure 4b). The distribution of large particles (>100 μm) measured using the UVP5 revealed similar distributions (Figure 4c). Increased concentrations of large particles were also observed in the frontal zone from 150 to 300 m, suggesting vertical transport of material from the surface to the mesopelagic zone beneath this feature (Figure 4c). In addition, qPCR amplification of *Trichodesmium* spp. *nifH* genes collected in sediment trap materials revealed an elevated (by more than an order of magnitude) *nifH* gene flux at 300 m in the frontal zone (4.7 ± 0.8 × 10^6 *nifH* gene copies m^{-2} d^{-1}) (Table 1)
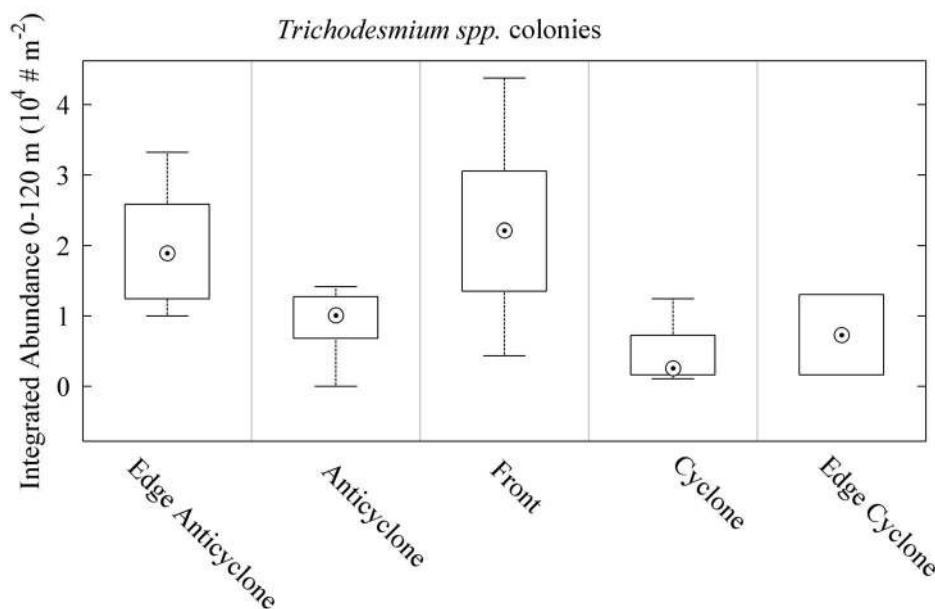

Figure 3. Integrated *Trichodesmium* spp. colony abundance (median, first, and third quartiles) between 0 and 120 m from the edge of the anticyclone and the edge of the cyclone.
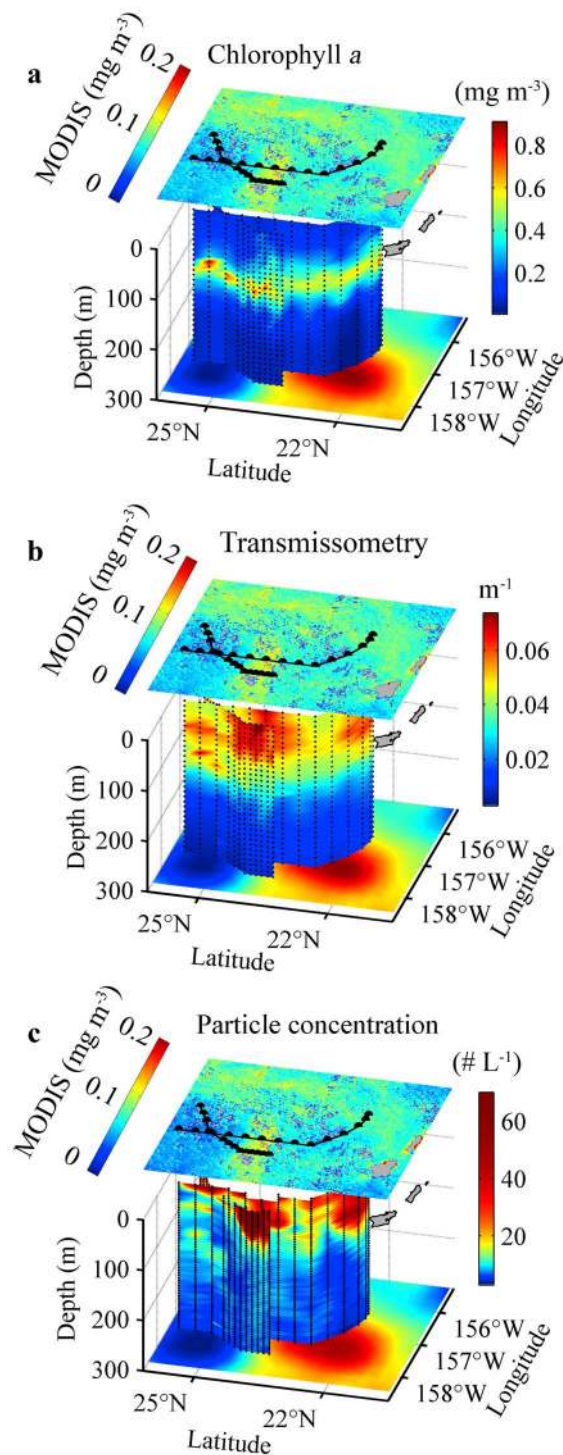
Figure 4. Three-dimensional representation of the 2 transects superimposed on (top) the MODIS-derived chlorophyll *a* measurements (8-day composite centered on 5 August 2008), and (bottom) the AVISO-derived sea surface height anomaly (6 August 2008). (a) Chlorophyll *a* obtained from continuous fluorescence profiles (0–300 m); note the two different scales for the transects and the chlorophyll *a* from MODIS. (b) Attenuation coefficient (m^{-1}) due to suspended particles as measured by transmissometry (0–300 m, λ = 660 nm, 25-cm path length). (c) Large (>100 μm) particle abundance from the UVP5.

compared to the cyclonic eddy ($1.9 \pm 0.9 \times 10^5$ *nifH* gene copies m^{-2} d^{-1}) (Table 1), reflecting different composition of sinking particles in the two regions. Finally, vertical transport of *Trichodesmium* spp. into the upper regions of the mesopelagic zone appeared more efficient in the frontal zone than in the cyclonic eddy ($56 \pm 10\%$, versus $31 \pm 10\%$, of sinking *Trichodesmium* spp. *nifH* genes captured in sediment traps at 150 m were transferred to 300 m, respectively).

[22] POC fluxes calculated from the UVP5 particle size distributions (equation (2)) [*Guidi et al.*, 2008] were similar to, though generally somewhat lower than, fluxes measured from the limited number of sediment traps, despite different assumptions and errors inherent to each technique (Table 1). Both sets of measurements revealed large spatial variability in carbon export. Sediment trap-derived POC flux at 150 m in the frontal zone was 1.8 times higher than in the cyclone. The higher spatial resolution of UVP5 flux estimates indicated fluxes 2.1 greater in the frontal zone than in the cyclonic eddy (11 versus 5.1 mgC m^{-2} d^{-1}; Figures 5a–5b; Table 1). Using sediment trap POC flux at 150 m, assuming a *Trichodesmium* spp. carbon content equal 42 pgC $cell^{-1}$ [*Goebel et al.*, 2008] and that one *nifH* gene corresponds to one *Trichodesmium* spp. cell, the contributions of
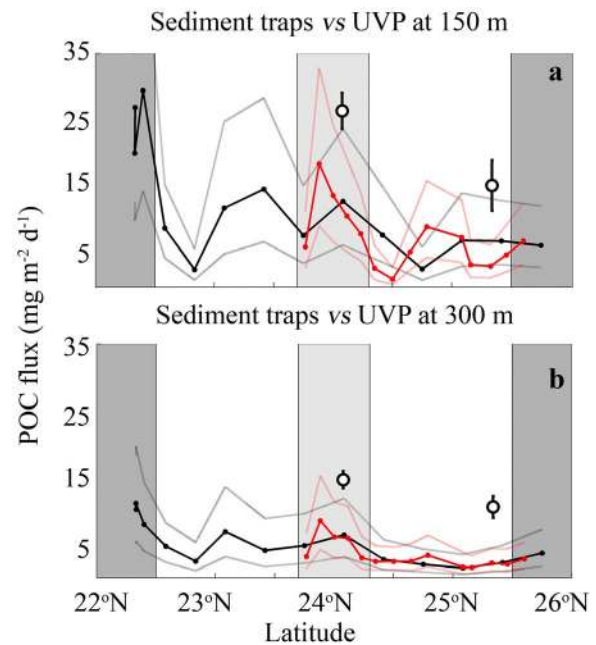

Figure 5. POC fluxes determined from sediment traps in the frontal zone and the center of cyclone (circle and bar indicating mean and standard deviation of replicate trap fluxes where *n* = 3), and POC flux estimations from UVP5-derived particle size distributions at (a) 150 m and (b) 300 m. The black curves are the estimates from the transect, while the red curves are derived from the short transect (cf. Figure 1). Solid lines are used for the median and dotted lines for extreme values calculated based on the uncertainties associated with the modeled POC. The leftmost gray area is the southern edge of the anticyclone, the central gray area is the frontal zone and the rightmost gray area is the northern edge of the cyclone.
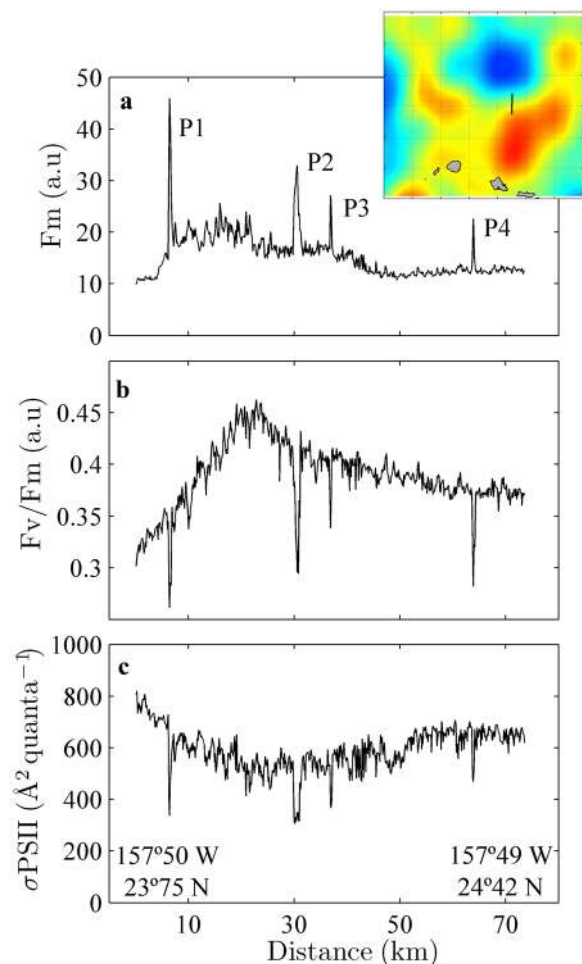
Figure 6. Fluorescence signals recorded by fast repetition rate fluorometry (FRRF) along a 70 km transect across the frontal zone (location of the transect represented by the black line over AVISO SSH anomaly, 6 August 2008); (a) amplitude of the fluorescence signal in arbitrary units (proxy for chlorophyll biomass), (b) the F_v/F_m signal in arbitrary units (proxy for the photosynthetic yield), and (c) the functional absorption cross section (proxy for photosynthetic light utilization). The peaks P1 and P2 correspond to the visual presence of *Trichodesmium* slicks in the surface waters. In addition, trichomes were visually detected in the sample chamber of the FRRF instrument at the location of peak P4.

Trichodesmium spp. to the POC flux in the front and the cyclone would be equal to 1.3% and 0.2%, respectively.

4. Discussion

[23] The OPEREX ecological and biogeochemical observations suggest that the elevated surface chlorophyll in the frontal region is associated with the presence of a *Trichodesmium* spp. bloom that occurred previous to or during the cruise. In contrast, several lines of evidence indicate that the elevated chlorophyll *a* concentration at the frontal boundary was not caused by a diatom bloom. First, there was no drawdown of the DSi inventories in the upper water column (Figure 2c) that would have been indicative of a past or ongoing diatom bloom. Second, fucoxanthin, a

diagnostic pigment for diatoms, was highest in the anticyclone, but low within both the frontal zone and the cyclone (Integrated 0–75 m: 628 ± 225, 335 ± 130, 391 ± 85 μg m^{-2}) (Table 1). No statistical difference (ANOVA; p > 0.01) was found in the integrated cell counts of any picoplankton group (bacterioplankton, *Prochlorococcus*, picophytoeukaryotes, *Synechococcus*) across the eddy field despite the observed increase of chlorophyll in the frontal zone (Table 1). Although the independent estimates of *Trichodesmium* spp. concentrations and fluxes cannot be compared to each other because of the different methods and units used (slides, UVP5, and sediment traps) (Table 1), all results showed the same trend of highest concentration/flux of *Trichodesmium* spp. in the high-chlorophyll frontal zone. A rough estimate of the contribution of *Trichodesmium* spp. to the frontal chlorophyll *a*, assuming 20–50 ngChl per colony for colonies made of 100–200 trichomes [*Carpenter et al.*, 2004], indicates that *Trichodesmium* spp. represented only 0.5–1.5% of the integrated 0–120 chlorophyll *a* in the frontal zone (~24–63 mgChl m^{-2} for 2.2 × 10^4 colonies m^{-2}). Picoplankton groups or *Trichodesmium* spp. contribution to the total chlorophyll cannot explain the frontal increase in chlorophyll *a* based on the ocean color data, suggesting a potential increase in the chlorophyll *a* to carbon ratios by non-*Trichodesdium* cells.

[24] Understanding whether the elevated concentrations of chlorophyll and *Trichodesmium* spp. biomass in the front resulted from biological processes (locally higher productivity) or physical processes (horizontal transport and accumulation of cells) may lend new insight into bloom dynamics in this region. The rate of chlorophyll-normalized photosynthetic carbon fixation in >2 μm plankton cells (P^B_{max} parameter) at 5 m showed no differences among the cyclone, anticyclone and frontal zones (9.7 ± 0.8, 10.5 ± 0.4, and 10.9 ± 0.7 mgC mgChl^{-1} h^{-1}, respectively), suggesting that locally enhanced production is not the cause. Alternatively large, buoyant phytoplankton cells or colonies, such as *Trichodesmium* spp., may have been advected into the frontal zone and accumulated in regions of convergent flow, enhancing chlorophyll *a* concentrations there. Such enhancement, however, cannot be explained solely by the advection of the chlorophyll *a*-bearing *Trichodesmium* spp. because of their insufficient numerical abundance.

[25] A complementary view on phytoplankton status can be derived from FRRF data [*Kolber et al.*, 1998] measured continuously across the frontal zone. The FRRF results indicated up to a twofold increase in the front surface chlorophyll *a* fluorescence signal (Figure 6a) and a coincident 20% increase in photosynthetic efficiency (F_v/F_m) (Figure 6b). This F_v/F_m increase occurred simultaneously with a 35% decrease in the functional absorption cross section compared to the background level (Figure 6c), indicative of the presence of large cells and colonies. These patterns were punctuated by sharp, 0.5–1.0 km wide fluorescence peaks corresponding to visual observations of surface patches of *Trichodesmium* spp. (Figure 6a). These narrow spatial peaks were characterized by smaller F_v/F_m values and a smaller functional absorption cross section at 470 nm (Figures 6b–6c) similar to those measured for the *Trichodesmium* spp. colonies collected in the frontal zone (data not shown).
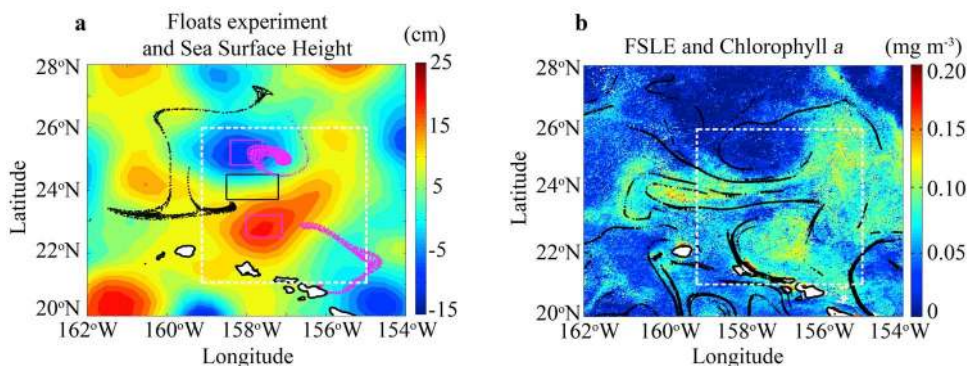
Figure 7. (a) Backward trajectory model designed to identify the source of the waters released in the cyclone and anticyclone (pink rectangles) and frontal zone (black rectangle). Floats were advected backward for 30 days using the AVISO-derived surface geostrophic velocities. (b) Finite-size Lyapunov exponents (FSLE) maxima superimposed on chlorophyll *a* from MODIS (8-day composite centered on 5 August 2008) representing the location of large stretching. White dashed rectangles delimit the area presented in Figure 4.

[26] The increase in the F_v/F_m observed in the transition zone (Figure 6b) indicates a local enhancement of photosynthetic efficiency, in contrast to the nearly constant ^{14}C-based P^B_{max} values across the eddy field. Moreover, there were changes in P-I relationships, as the chlorophyll-normalized slope of the P-I curves was about 20%–30% higher in the frontal zone (0.057 mgC mgChl^{-1} h^{-1} μE^{-1}) than in the anticyclone and cyclone zones (0.035 and 0.046 mgC mgChl^{-1} h^{-1} μE^{-1}, respectively), consistent with a local increase in F_v/F_m, and indicative of higher primary production under subsaturating irradiances. Indeed, the P^B_{max} measured at the depth of DCML in the frontal zone (5.24 mgC mgChl^{-1} h^{-1}) was significantly higher than that measured in the DCML of the anticyclone (2.56 mgC mgChl^{-1} h^{-1}) and similar to that observed in the DCML of the cyclone (6.02 mgC mgChl^{-1} h^{-1}), where the upwelling of nitrate-rich waters (Figure 4a) may have been responsible for higher level of primary production.

[27] The increased P^B_{max} at the depth of the DCML and surface increase of F_v/F_m in the frontal zone are consistent with the increased concentration of *Trichodesmium* spp. in the frontal zone, supplying new nitrogen via nitrogen fixation. Such nitrogen fixation would contribute to the local biomass increase of the entire phytoplankton community. In a similar manner, upwelling of nitrate could have stimulated biomass production at the bottom of the euphotic layer in the cyclonic eddy (Figure 4a), possibly explaining the higher F_v/F_m signal observed there. None of these possibilities accounts for the uniform surface values of P^B_{max} across the region.

[28] The different sampling rates of the two techniques could explain the differences. Photosynthesis versus irradiance (P-I) data were collected at much lower spatial resolution (at only 3 stations, with only 1 station in the frontal zone) than FRRF data (continuous). As a result, the P^B_{max} values may be aliased by the unresolved, high-frequency features observed in the F_v/F_m signal (Figure 6b). Interestingly, the total integrated (0–100 m) POC was also fairly constant across the eddy field (only 3 stations were sampled) whereas particle concentrations from both transmissivity and UVP5 showed strong spatial variability (high resolution sampling). As with the FRRF and ^{14}C primary production measurements, differences in sampling resolution could explain this discrepancy. In addition, samples for total POC measurements were from 4 L of filtered water prescreened through a 200 μm mesh to remove any zooplankton contribution. This process will predominantly exclude larger particles such as *Trichodesmium* spp. colonies and further increase differences between optical estimates and biogeochemical measurement of POC stocks. Because of these different results, our data set could not provide clear evidence that the accumulation of *Trichodesmium* spp. and the increase of chlorophyll in the frontal zone resulted from an increase in primary production. However, our results stress the importance of performing more thorough comparisons between optical and biogeochemical measurements, such as the FRRF signatures and P-I data at the submesocale level, in future studies to improve the interpretation of the differences between these two different spatial scales and gain better understanding on bloom dynamics in the NPSG.

[29] We also investigated the importance of physical processes on the observed biological spatial variability. Backward trajectories calculated using surface geostrophic velocities from the AVISO altimetry revealed that the water flowing into the frontal region did not originate from either the cyclone or the anticyclone (Figure 7a). Waters in the frontal region came mostly from the west, northwest and north following the flow pattern defined by the dipole. The source waters for the inner core of the cyclone and the anticyclone also differed (Figure 7a). The former were carried along as part of the westward propagation of the cyclone while the latter generally originated in the southeast. Because the AVISO altimetry does not resolve the Hawaiian Islands, the trajectories for the anticyclone core potentially could have errors. The maxima in FSLE, which are associated with areas undergoing rapid stretching, for the week centered on 5 August 2008 aligned well with the satellite-derived chlorophyll *a* distributions (Figure 7b), suggesting that the structure of the bloom and the distribution of phytoplankton biomass appear to be controlled by horizontal stirring [*Calil et al.*, 2011].
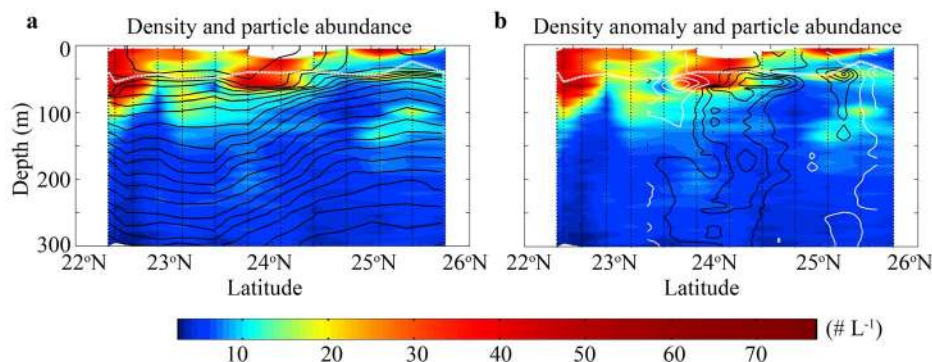
Figure 8. Large particle (>100 μm) abundance from the UVP5 corresponding to the transect in Figure 4c with the mixed layer depth represented by the white dashed line: (a) contour plot of the density field showing particle accumulation on isopycnals; (b) contour plot of the density anomalies showing the locations of the downwelling water (black contour) and the upwelling water (white contour).

[30] The large stretching in the frontal region between the two eddies has dynamical consequences as it intensifies the existing lateral subsurface temperature gradient. In situ physical observations show a subsurface mesoscale front present between the two eddies, with the isopycnals trending upwards toward the central part of the cyclone and an intensifying density front in the upper 60 m between 24.25°N and 24.75°N (Figure 8a). The intensification of this density front appeared to derive from stretching induced by the two eddies. The largest FSLE values were approximately 0.1 d^{-1} (black lines in Figure 7b), which yield a time-scale of frontal intensification of approximately 3 days.

[31] The confluence and sharpening of surface density fronts can result in a breakdown of the thermal wind balance, the geostrophic balance between the horizontal density gradients and the vertical shear of the horizontal velocity [*Mahadevan and Tandon*, 2006]. In order to restore this balance, ageostrophic secondary circulations usually are generated on a plane perpendicular to the front, a process known as surface frontogenesis [*Lapeyre and Klein*, 2006]. To evaluate if frontogenesis produced vertical velocities, we used a scaling of the omega equation [*Legal et al.*, 2007] in which vertical velocities are inversely proportional to density anomalies ($\delta\rho$), here defined as deviations from the average mixed layer value of the density in the transect; of course any calculation involving lateral gradient is resolution dependent. The calculation of $\delta\rho$ reveals the presence of a prominent positive density anomaly (0.5 kg m^{-3}) between 23.8°N and 24.6°N, which is indicative of frontogenetically generated downwelling (surface convergent flow) of ~20 m d^{-1} (Figure 8b, black contour).

[32] Consistent with this estimation of water movement, the observed particle distribution data collected by the UVP5 and flux measurements from sediment trap observations indicated enhanced POC export occurring in these downwelling regions. For particles to accumulate in the convergent flow of the front they must be positively buoyant, which is the case for *Trichodesmium* spp., but these particles could still be carried to depth if the local downwelling velocity exceeded the upward velocity due to buoyancy. *Trichodesmium* spp. ascent and sinking rates have been estimated to vary between −216 (sinking) and +260 m d^{-1}

(ascent) with average upward motion of 3 m d^{-1} [*Walsby*, 1978; *Villareal and Carpenter*, 1990]. Given this large range, the frontal downwelling water of 20 m d^{-1} could take some *Trichodesmium* spp. colonies, as well as the other sinking particles, to depth when it exceeds their ascent rates. Consequently, vertical water movements may enhance the export of POC from the surface into the ocean's interior. Such a particle transport mechanism is supported by previous results from modeling [*Lima et al.*, 2002], and observations [*Guidi et al.*, 2007; *Stemmann et al.*, 2008]. The mixed layer depth did not seem to act as a barrier to particle export, except at 25–25.5°N, where the deep particle maximum appeared to be trapped by this feature (Figures 8a–8b).

[33] The increased particle flux in the frontal zone could also result from increased grazing as a consequence of the particle accumulation in the surface layer. However, this was not supported by results from the UVP5 images, which showed low integrated concentrations of grazers in the upper 120 m at the anticyclone and frontal zones (698 ± 517 and 722 ± 712 copepods m^{-2}, respectively) and higher within the cyclone (1312 ± 586 copepods m^{-2}). Unfortunately data on zooplankton community were limited to the UVP5 images and would need to be verified by targeted net tows in future studies.

5. Conclusions

[34] The elevated chlorophyll *a*, particle concentrations, and export flux measured in the frontal region within the cyclonic-anticyclonic dipole are consistent with mesoscale and submesoscale physical processes influencing the biological ones. Horizontal stirring appears to have caused surface convergence within the mesoscale frontal zone, which in turn increased concentrations of buoyant particles, such as *Trichodesmium* spp., and stimulated particle downward transport. The elevated concentrations of active nitrogen fixers, potentially bringing new nitrogen into the environment, could have stimulated total primary production. Data for this enhancement were contradictory, with FRRF supporting it and ^{14}C-based measurements only partially doing so. The ^{14}C-based measurements suggest that the possible enhancement of primary production in the frontal zone was limited to depths where irradiance

decreases to sub-saturating levels. The mechanisms driving the surface variability in *Trichodesmium* spp. and chlorophyll *a* distribution remain uncertain and need to be investigated further. Analyses of the water displacements, particle size distributions and fluxes suggest that surface frontogenesis induced by the stretching of the flow may have generated downwelling velocities sufficiently strong to promote particle export. Some of these particles could have included colonies of *Trichodesmium* spp. when their ascent rates were less than the downwelling velocity of the water (20 m d^{-1}). Therefore, POC export may have been a consequence of multiple processes, including passive sedimentation and active export (downwelling water).

[35] Mesoscale eddies, filaments, and fronts are ubiquitous in the ocean and have been shown to play important roles in controlling primary production [*Falkowski et al.*, 1991; *McGillicuddy et al.*, 1998; *Oschlies and Garçon*, 1998; *Allen et al.*, 2005]. The mechanisms described in this study off Hawaii may apply in other mesoscale features in many regions of the global ocean and need to be assessed if we are to understand and quantify global carbon export. Our results indicate that physical dynamics associated with submesoscale and mesoscale fields may play an important role in particle accumulation and facilitate carbon export out of the upper ocean. Our Lagrangian diagnostics were able to capture the filamentation tendency driven by the interaction of the two eddies. The use of biogeochemical proxies (FRRF and UVP5) allowed high frequency monitoring of the fluorescence signals and the particle (>100 μm) concentration and confirmed a high degree of spatial variability. However, classical biogeochemical measurements (^{14}C-based primary production, POC, DSi, N+N, flow cytometry counts) did not always agree with these observations, possibly because of different measurement sampling rates and spatial/temporal resolutions. The OPEREX cruise highlights the need to combine high-resolution biogeochemical data sets to match high frequency measurements from instruments such as the FRRF and UVP5. This approach will lead to a better understanding of the links between the surface and subsurface biogeochemistry, and the physics at the submesoscale level. In particular, studies seeking to resolve the magnitude and variability associated with POC export may need to account for small-scale spatial variability in physical dynamics as controls on carbon export. To that end, sampling strategies that better resolve small-scale variability using a combination of towed and autonomous platforms (e.g., floats, gliders, AUVs) coupled with high-resolution modeling and remote sensing should be pursued.

References

Abraham, E. R. (1998), The generation of plankton patchiness by turbulent stirring, *Nature*, *391*(6667), 577–580, doi:10.1038/35361.

Alldredge, A. L., and C. Gotschalk (1988), In situ settling behavior of marine snow, *Limnol. Oceanogr.*, *33*(3), 339–351, doi:10.4319/lo.1988.33.3.0339.

Allen, J. T., et al. (2005), Diatom carbon export enhanced by silicate upwelling in the northeast Atlantic, *Nature*, *437*(7059), 728–732, doi:10.1038/nature03948.

Benavides, M., N. S. R. Agawin, J. Aristegui, P. Ferriol, and L. J. Stal (2011), Nitrogen fixation by *Trichodesmium* and small diazotrophs in the subtropical northeast Atlantic, *Aquat. Microb. Ecol.*, *65*(1), 43–53, doi:10.3354/ame01534.

Calil, P. H. R., and K. J. Richards (2010), Transient upwelling hot spots in the oligotrophic North Pacific, *J. Geophys. Res.*, *115*, C02003, doi:10.1029/2009JC005360.

Calil, P. H. R., S. C. Doney, K. Yumimoto, K. Eguchi, and T. Takemura (2011), Episodic upwelling and dust deposition as bloom triggers in low-nutrient, low-chlorophyll regions, *J. Geophys. Res.*, *116*, C06030, doi:10.1029/2010JC006704.

Carpenter, E. J. (1983), Physiology and ecology of marine planktonic *Oscillatoria* (*Trichodesmium*), *Mar. Biol. Lett.*, *4*(2), 69–85.

Carpenter, E. J., A. Subramaniam, and D. G. Capone (2004), Biomass and primary productivity of the cyanobacterium *Trichodesmium* spp. in the tropical N Atlantic ocean, *Deep Sea Res., Part I*, *51*(2), 173–203, doi:10.1016/j.dsr.2003.10.006.

Church, M. J., B. D. Jenkins, D. M. Karl, and J. P. Zehr (2005), Vertical distributions of nitrogen-fixing phylotypes at Stn ALOHA in the oligotrophic North Pacific Ocean, *Aquat. Microb. Ecol.*, *38*(1), 3–14, doi:10.3354/ame038003.

Church, M. J., C. Mahaffey, R. M. Letelier, R. Lukas, J. P. Zehr, and D. M. Karl (2009), Physical forcing of nitrogen fixation and diazotroph community structure in the North Pacific subtropical gyre, *Global Biogeochem. Cycles*, *23*, GB2020, doi:10.1029/2008GB003418.

d'Ovidio, F., V. Fernandez, E. Hernandez-Garcia, and C. Lopez (2004), Mixing structures in the Mediterranean Sea from finite-size Lyapunov exponents, *Geophys. Res. Lett.*, *31*(17), L17203, doi:10.1029/2004GL020328.

d'Ovidio, F., S. De Montec, S. Alvain, Y. Dandonneau, and M. Lévy (2010), Fluid dynamical niches of phytoplankton types, *Proc. Natl. Acad. Sci. U. S. A.*, *107*(43), 18,366–18,370, doi:10.1073/pnas.1004620107.

Davis, C. S., and D. J. McGillicuddy (2006), Transatlantic abundance of the N$_2$-fixing colonial cyanobacterium *Trichodesmium*, *Science*, *312*(5779), 1517–1520, doi:10.1126/science.1123570.

Doney, S. C., D. M. Glover, S. J. McCue, and M. Fuentes (2003), Mesoscale variability of Sea-viewing Wide Field-of-view Sensor(SeaWiFS) satellite ocean color: Global patterns and spatial scales, *J. Geophys. Res.*, *108*(C2), 3024, doi:10.1029/2001JC000843.

Dore, J. E., R. M. Letelier, M. J. Church, R. Lukas, and D. M. Karl (2008), Summer phytoplankton blooms in the oligotrophic North Pacific Subtropical Gyre: Historical perspective and recent observations, *Prog. Oceanogr.*, *76*(1), 2–38, doi:10.1016/j.pocean.2007.10.002.

Emerson, S., P. Quay, D. Karl, C. Winn, L. Tupas, and M. Landry (1997), Experimental determination of the organic carbon flux from open-ocean surface waters, *Nature*, *389*(6654), 951–954, doi:10.1038/40111.

Falkowski, P. G., D. Ziemann, Z. Kolber, and P. K. Bienfang (1991), Role of eddy pumping in enhancing primary production in the ocean, *Nature*, *352*(6330), 55–58, doi:10.1038/352055a0.

Fong, A. A., D. M. Karl, R. Lukas, R. M. Letelier, J. P. Zehr, and M. J. Church (2008), Nitrogen fixation in an anticyclonic eddy in the oligotrophic North Pacific Ocean, *ISME J.*, *2*(6), 663–676, doi:10.1038/ismej.2008.22.

Goebel, N. L., C. A. Edwards, B. J. Carter, K. M. Achilles, and J. P. Zehr (2008), Growth and carbon content of three different-sized diazotrophic cyanobacteria observed in the subtropical North Pacific, *J. Phycol.*, *44*(5), 1212–1220, doi:10.1111/j.1529-8817.2008.00581.x.

Guidi, L., L. Stemmann, L. Legendre, M. Picheral, L. Prieur, and G. Gorsky (2007), Vertical distribution of aggregates (>110 μm) and mesoscale activity in the northeastern Atlantic: Effects on the deep vertical export of surface carbon, *Limnol. Oceanogr.*, *52*(1), 7–18, doi:10.4319/lo.2007.52.1.0007.

Guidi, L., G. A. Jackson, L. Stemmann, J. C. Miquel, M. Picheral, and G. Gorsky (2008), Relationship between particle size distribution and flux in the mesopelagic zone, *Deep Sea Res., Part I*, *55*, 1364–1374, doi:10.1016/j.dsr.2008.05.014.

Jackson, G. A., R. Maffione, D. K. Costello, A. L. Alldredge, B. E. Logan, and H. G. Dam (1997), Particle size spectra between 1 μm and 1 cm at Monterey Bay determined using multiple instruments, *Deep Sea Res., Part I*, *44*(11), 1739–1767, doi:10.1016/S0967-0637(97)00029-0.

Johnson, K. S., S. C. Riser, and D. M. Karl (2010), Nitrate supply from deep to near-surface waters of the North Pacific subtropical gyre, *Nature*, *465*(7301), 1062–1065, doi:10.1038/nature09170.

Karl, D. M., R. R. Bidigare, and R. M. Letelier (2001), Long-term changes in plankton community structure and productivity in the North Pacific Subtropical Gyre: The domain shift hypothesis, *Deep Sea Res., Part II*, *48*(8–9), 1449–1470, doi:10.1016/S0967-0645(00)00149-1.

Klein, P., and G. Lapeyre (2009), The oceanic vertical pump induced by mesoscale and submesoscale turbulence, *Annu. Rev. Mar. Sci.*, *1*(1), 351–375, doi:10.1146/annurev.marine.010908.163704.

Knauer, G. A., J. H. Martin, and K. W. Bruland (1979), Fluxes of particulate carbon, nitrogen, and phosphorus in the upper water column of the northeast Pacific, *Deep Sea Res.*, *26*(1), 97–108, doi:10.1016/0198-0149(79)90089-X.

Kolber, Z. S., O. Prasil, and P. G. Falkowski (1998), Measurements of variable chlorophyll fluorescence using fast repetition rate techniques: Defining methodology and experimental protocols, *Biochim. Biophys. Acta, Bioenerg.*, *1367*(1–3), 88–106, doi:10.1016/S0005-2728(98)00135-2.

Lapeyre, G., and P. Klein (2006), Impact of the small-scale elongated filaments on the oceanic vertical pump, *J. Mar. Res.*, *64*(6), 835–851, doi:10.1357/002224006779698369.

LaRoche, J., and E. Breitbarth (2005), Importance of the diazotrophs as a source of new nitrogen in the ocean, *J. Sea Res.*, *53*(1–2), 67–91, doi:10.1016/j.seares.2004.05.005.

Legal, C., P. Klein, A. M. Treguier, and J. Paillet (2007), Diagnosis of the vertical motions in a mesoscale stirring region, *J. Phys. Oceanogr.*, *37*(5), 1413–1424, doi:10.1175/JPO3053.1.

Lehahn, Y., F. d'Ovidio, M. Lévy, and E. Heifetz (2007), Stirring of the northeast Atlantic spring bloom: A Lagrangian analysis based on multisatellite data, *J. Geophys. Res.*, *112*, C08005, doi:10.1029/2006JC003927.

Letelier, R. M., and D. M. Karl (1996), Role of *Trichodesmium* spp. in the productivity of the subtropical North Pacific Ocean, *Mar. Ecol. Prog. Ser.*, *133*(1–3), 263–273, doi:10.3354/meps133263.

Letelier, R. M., D. M. Karl, M. R. Abbott, P. Flament, M. Freilich, R. Lukas, and T. Strub (2000), Role of late winter mesoscale events in the biogeochemical variability of the upper water column of the North Pacific Subtropical Gyre, *J. Geophys. Res.*, *105*(C12), 28,723–28,739, doi:10.1029/1999JC000306.

Lévy, M., P. Klein, and A. M. Treguier (2001), Impact of sub-mesoscale physics on production and subduction of phytoplankton in an oligotrophic regime, *J. Mar. Res.*, *59*(4), 535–565, doi:10.1357/002224001762842181.

Lévy, M., P. Klein, and M. Ben Jelloul (2009), New production stimulated by high-frequency winds in a turbulent mesoscale eddy field, *Geophys. Res. Lett.*, *36*, L16603, doi:10.1029/2009GL039490.

Lima, I. D., D. B. Olson, and S. C. Doney (2002), Biological response to frontal dynamics and mesoscale variability in oligotrophic environments: Biological production and community structure, *J. Geophys. Res.*, *107*(C8), 3111, doi:10.1029/2000JC000393.

Mahadevan, A., and D. Archer (2000), Modeling the impact of fronts and mesoscale circulation on the nutrient supply and biogeochemistry of the upper ocean, *J. Geophys. Res.*, *105*(C1), 1209–1225, doi:10.1029/1999JC900216.

Mahadevan, A., and A. Tandon (2006), An analysis of mechanisms for submesoscale vertical motion at ocean fronts, *Ocean Modell.*, *14*(3–4), 241–256, doi:10.1016/j.ocemod.2006.05.006.

Martin, J. H., G. A. Knauer, D. M. Karl, and W. W. Broenkow (1987), VERTEX: Carbon cycling in the northeast Pacific, *Deep Sea Res.*, *34*(2A), 267–285.

McCave, I. N. (1984), Size spectra and aggregation of suspended particles in the deep ocean, *Deep Sea Res., Part I*, *31*(4), 329–352, doi:10.1016/0198-0149(84)90088-8.

McGillicuddy, D. J., A. R. Robinson, D. A. Siegel, H. W. Jannasch, R. Johnson, T. Dickeys, J. McNeil, A. F. Michaels, and A. H. Knap (1998), Influence of mesoscale eddies on new production in the Sargasso Sea, *Nature*, *394*(6690), 263–266, doi:10.1038/28367.

McGillicuddy, D. J., L. A. Anderson, S. C. Doney, and M. E. Maltrud (2003), Eddy-driven sources and sinks of nutrients in the upper ocean: Results from a 0.1° resolution model of the North Atlantic, *Global Biogeochem. Cycles*, *17*(2), 1035, doi:10.1029/2002GB001987.

Moore, J. K., S. C. Doney, K. Lindsay, N. Mahowald, and A. F. Michaels (2006), Nitrogen fixation amplifies the ocean biogeochemical response to decadal timescale variations in mineral dust deposition, *Tellus, Ser. B*, *58*(5), 560–572, doi:10.1111/j.1600-0889.2006.00209.x.

Niewiadomska, K., H. Claustre, L. Prieur, and F. d'Ortenzio (2008), Submesoscale physical-biogeochemical coupling across the Ligurian Current (northwestern Mediterranean) using a bio-optical glider, *Limnol. Oceanogr.*, *53*, 2210–2225, doi:10.4319/lo.2008.53.5_part_2.2210.

Oschlies, A., and V. Garçon (1998), Eddy-induced enhancement of primary production in a model of the North Atlantic Ocean, *Nature*, *394*(6690), 266–269, doi:10.1038/28373.

Picheral, M., L. Guidi, L. Stemmann, D. M. Karl, G. Iddaoud, and G. Gorsky (2010), The Underwater Vision Profiler 5: An advanced instrument for high spatial resolution studies of particle size spectra and zooplankton, *Limnol. Oceanogr. Methods*, *8*, 462–473, doi:10.4319/lom.2010.8.462.

Platt, T., C. L. Gallegos, and W. G. Harrison (1980), Photoinhibition of photosynthesis in natural assemblages of marine-phytoplankton, *J. Mar. Res.*, *38*(4), 687–701.

Redfield, A. C., B. H. Ketchum, and F. A. Richards (1963), The influence of organisms on the composition of sea-water, in *The Composition of Sea-Water Comparative and Descriptive Oceanography*, edited by M. N. Hill, pp. 26–77, John Wiley, New York.

Stemmann, L., L. Prieur, L. Legendre, I. Taupier-Letage, M. Picheral, L. Guidi, and G. Gorsky (2008), Effects of frontal processes on marine aggregate dynamics and fluxes: An interannual study in a permanent geostrophic front (NW Mediterranean), *J. Mar. Syst.*, *70*(1–2), 1–20, doi:10.1016/j.jmarsys.2007.02.014.

Villareal, T. A., and E. J. Carpenter (1990), Diel buoyancy regulation in the marine diazotrophic cyanobacterium *Trichodesmium thiebautii*, *Limnol. Oceanogr.*, *35*(8), 1832–1837, doi:10.4319/lo.1990.35.8.1832.

Walsby, A. E. (1978), Properties and buoyancy-providing role of gas vacuoles in *Trichodesmium ehrenberg*, *Br. Phycol. J.*, *13*(2), 103–116, doi:10.1080/00071617800650121.

White, A. E., Y. H. Spitz, and R. M. Letelier (2007), What factors are driving summer phytoplankton blooms in the North Pacific Subtropical Gyre?, *J. Geophys. Res.*, *112*(C12), C12006, doi:10.1029/2007JC004129.

Wilson, C. (2003), Late summer chlorophyll blooms in the oligotrophic North Pacific Subtropical Gyre, *Geophys. Res. Lett.*, *30*(18), 1942, doi:10.1029/2003GL017770.

Zhang, H., and S. J. Lin (2005), Development of a *cob*-18S rRNA gene real-time PCR assay for quantifying *Pfiesteria shumwayae* in the natural environment, *Appl. Environ. Microbiol.*, *71*(11), 7053–7063, doi:10.1128/AEM.71.11.7053-7063.2005.